


Evaporation Flow Heat Transfer Characteristics of Stainless Steel and Copper Enhanced Tubes

Xu Wang ^{1,*}, David John Kukulka ^{2,*} , Xiang-Zeng Liu ³, Wei Feng ³, Xiao-Bo Wang ³, Wei Li ⁴ and Ze-Peng Wang ³

¹ College of Energy and Transportation Engineering, Inner Mongolia Agricultural University, 306 Zhaowuda Road, Hohhot 010018, China

² Department of Mechanical Engineering Technology, State University of New York College at Buffalo, 1300 Elmwood Avenue, Buffalo, NY 14222, USA

³ Department of Mechanical and Electrical Engineering, Qingdao University of Science and Technology, 99 Songling Road, Qingdao 266061, China

⁴ Department of Energy Engineering, Zhejiang University, 38 Zheda Road, Hangzhou 310027, China

* Correspondence: yiqiyihui_wang@163.com (X.W.); kukulkdj@buffalostate.edu (D.J.K.)

Abstract: An experimental study was undertaken to study the tube-side evaporation heat transfer characteristics of enhanced tubes and compare their performance with that of smooth tubes. These experiments were conducted in order to determine how R410a evaporates inside smooth and enhanced tubes; for a saturation temperature of 279.15 K; with mass flux values that ranged from 50 to 250 kg/(m²·s); for an inlet quality of 0.2 and outlet quality of 0.8. Enhanced tubes evaluated include herringbone (HB) and helix (HX) designs with microgrooves, composite herringbone dimple (HB/D), composite herringbone hydrophobic (HB/HY), and composite EHT (multiple enhancement character) tubes. Experimental results show that the evaporation heat-transfer coefficient in the Cu-EHTb tube was the highest; its performance was closely related to the increased number of nucleation points that are found inside the tube; however, the performance of the SS-EHT-HB/D was not significantly higher than that of a smooth tube. The best overall capacity for evaporative heat transfer is shown in the SS-EHT-HB/HY and SS-EHT-HX tubes; the SS-EHT-HB/D, Cu-EHTa, and Cu-EHTb tubes had the worst overall capacity among all the tested tubes. Additionally, it was determined that previously reported smooth tube models to determine the evaporation heat transfer coefficient can accurately predict the heat transfer inside a smooth tube. However, when trying to utilize smooth tube models for enhanced tubes, the deviation between experimentally determined heat transfer coefficient (HTC) values and those predicted when using smooth tube models to predict enhanced tube results is $\pm 30\%$; therefore, smooth tube models are not applicable for use with enhanced tubes. Smooth tube models were modified, and after correction, the deviation between experimentally determined heat transfer coefficient (HTC) values and those predicted when using the modified model for use with enhanced tubes is $\pm 10\%$. Finally, the effect of the thermal resistance of the tube wall on the overall heat transfer coefficient of a stainless steel-enhanced tube is significant and cannot be overlooked.

Keywords: enhanced tube; evaporation; heat transfer coefficient; correlations; thermal resistance



Citation: Wang, X.; Kukulka, D.J.; Liu, X.-Z.; Feng, W.; Wang, X.-B.; Li, W.; Wang, Z.-P. Evaporation Flow Heat Transfer Characteristics of Stainless Steel and Copper Enhanced Tubes. *Energies* **2023**, *16*, 2331. <https://doi.org/10.3390/en16052331>

Academic Editor: Feng Zhang

Received: 19 January 2023

Revised: 4 February 2023

Accepted: 22 February 2023

Published: 28 February 2023



Copyright: © 2023 by the authors. Licensee MDPI, Basel, Switzerland. This article is an open access article distributed under the terms and conditions of the Creative Commons Attribution (CC BY) license (<https://creativecommons.org/licenses/by/4.0/>).

1. Introduction

Passive enhanced heat transfer technology (which includes enhanced surface design) can significantly improve heat transfer performance in heat exchangers while not significantly increasing the pressure drop. As a result, there is a great deal of research interest in studying the performance of micro-finned tubes in refrigeration and air conditioning applications. Scholars have long been interested in the effect that fins (fin shape and related geometric structure parameters) have on the flow boiling heat transfer performance in micro-finned tubes. Kim et al. [1] investigated the effect that a micro-finned tube surface has on the boiling heat transfer performance for horizontal flows. They point out that as

the diameter increases, the heat transfer enhancement performance of micro-finned tubes outperforms smooth tubes. Wellsandt et al. [2] showed that the heat transfer coefficient (HTC) of a Y-shaped enhancement in micro-finned tubes is slightly higher than the HTC of the more traditional micro-finned tubes that have a spiral design; however, there is a slightly higher pressure drop in the Y-shaped tubes. Wu et al. [3] experimentally compared the flow boiling heat transfer performance of enhanced heat transfer tubes (5 mm external diameter tube) with five different micro-fin structures. The experimental results show that micro-finned tubes with fin heights of 0.15 mm and fin apex angles of 25° and 30° produce the best heat transfer performance at mass flux rates less than 400 kg/(m²·s). Yang et al. [4] proposed an improved flow pattern diagram for internal flows in horizontal micro-finned tubes; they found that the transition to annular flow occurs earlier in enhanced tubes than in smooth tubes. Rollmann et al. [5] developed a novel pressure drop correlation based on pressure drop data (for R407c and R410a) in micro-finned tubes.

The experimental performance evaluation of flow boiling heat transfer in enhanced tubes and the understanding of the boiling mechanism in enhanced tubes with different enhancement surfaces have become important topics with the recent development of new three-dimensional enhanced tubes. According to Webb et al. [6], three-dimensional enhanced tubes can increase surface area, increase nucleation sites, promote fluid mixing, generate secondary flows, create boundary layer separation, and increase turbulence intensity; all these factors make three-dimensional enhanced tubes an important consideration when evaluating alternatives to improve heat transfer. Vicente et al. [7] investigated syphon bellows at low Reynolds numbers. Kukulka et al. [8] investigated various EHT-enhanced tubes, and single-phase results show the heat transfer performance of the EHT-enhanced tubes was improved by more than 500%. These tubes produced an earlier transition to turbulence, occurring approximately when the Reynolds number was near 1000. Guo et al. [9] evaluated several enhanced tubes and found that the three-dimensional EHT tubes produced the largest evaporation heat transfer coefficient. This is the result of the enhanced surface structure of the EHT tube, which provides more nucleation sites for the evaporation exchange process. Additionally, the enhanced structure also produces a more intense disturbance at the two-phase flow interface and disrupts the boundary layer. Additionally, they found that the boiling heat transfer coefficient (HTC) for saturated flows in a Y-shaped micro-finned tube is only slightly greater than the HTC of a smooth tube. Kukulka et al. [10] experimentally studied the evaporation and condensation heat transfer characteristics of 1EHT (three-dimensional enhanced structure) tubes and compared the results to smooth tubes. Results showed that the 1EHT tube can provide approximately two times the evaporation heat transfer coefficient that is produced in smooth tubes; this confirms the importance of considering three-dimensional structures for use in flow boiling heat transfer tubes. According to Shafae et al. [11], the heat transfer coefficient of enhanced heat transfer tubes is approximately two times greater than the HTC produced in smooth tubes for the same conditions; however, there is a 7–103% increase in pressure drop (when compared to smooth tubes). Li et al. [12] produced an experimental system for measuring the tube-side heat transfer coefficient. They found improved performance in the EHT tube for low mass flux rates and low qualities; however, at high mass flux rates and high qualities, the enhanced surface did not produce as much improvement.

The evaporation heat transfer performance of three-dimensionally enhanced tubes is important in the design and development of heat transfer systems and equipment. The heat transfer coefficient of the enhanced tube is larger than that of the smooth tube; however, both heat transfer and pressure loss must be considered in order to determine true performance. Additionally, it is difficult to rely solely on a theoretical analysis or only a numerical analysis in order to determine performance in enhanced tubes. Experimental research is required to determine the heat transfer performance of enhanced tubes; additionally, the development of an enhanced tube performance model (based upon experimental data) that can be used to aid in the design of heat transfer devices must be validated using experimental data. Smooth, herringbone microgrooves (SS-EHT-HB), spiral microgrooves

(SS-EHT-HX), herringbone dimples (SS-EHT-HB/D), hydrophobic herringbones (SS-EHT-HB/HY), and three-dimensional EHT enhanced tubes are evaluated over a wide range of conditions in this study, and evaporation heat transfer performance is discussed.

2. Experimental Details

Figure 1 details the experimental apparatus used in this study. Additional details of the experimental setup and procedure are found in [13–15]. Figure 2 provides the surface map and parameters of the various enhanced surfaces studied here; Table 1 summarizes the main surface parameters of the tubes. Images of the enhanced surfaces are presented in Figure 3.

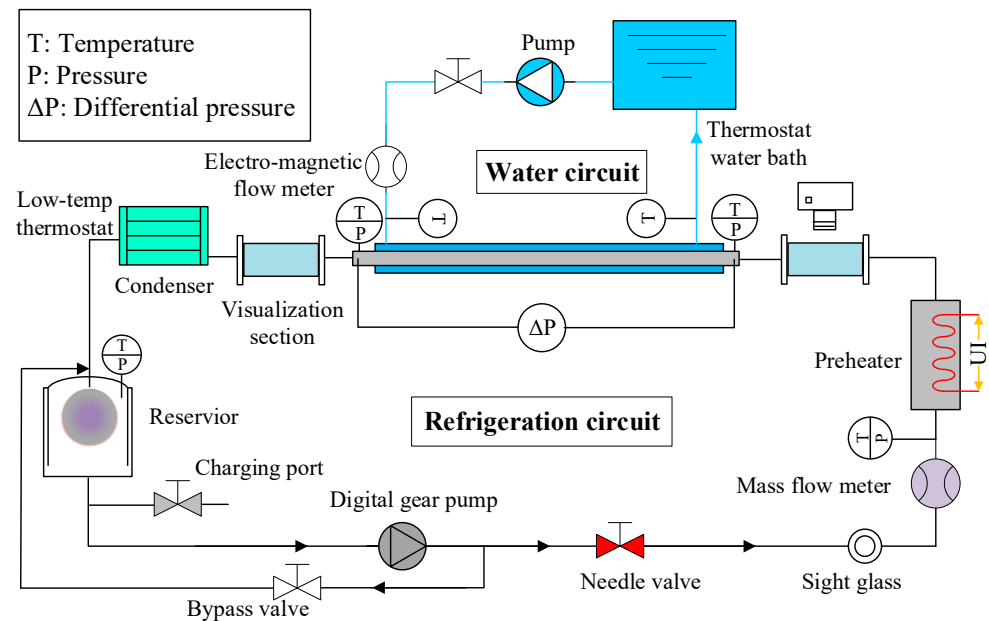


Figure 1. Schematic diagram of the experimental setup.

Experimental conditions used in this investigation include: R410a refrigerant; a saturation temperature of 6 °C; mass flux values that range from 50 to 250 kg/(m²·s); and an inlet vapor quality of 0.2 and an outlet vapor quality of 0.8. There are six test points for each type of tube. Each test point is repeated three times. The deviation between the heat transfer coefficient and pressure loss of the three repeated tests is less than 5%. Moffat [16] describes how to calculate the uncertainty (%) of directly measured and indirectly obtained parameters, and Table 2 summarizes the maximum relative errors of the measurements and calculated parameters. The maximum relative error of the HTC is calculated to be ±11.32%.

Table 1. Physical measurements of the enhancement patterns used in the various tubes.

Parameters	SS-EHT-HX	SS-EHT-HB	SS-EHT-HB/D	Cu-EHTa	Cu-EHTb
Dimple/fin height, mm	1.14	0.08	1.21	1.71	1.71
Dimple/fin pitch, mm	5	0.8	4	—	—
Dimple/fin width, mm	2.3	0.31	3.51	—	—
Helix angle, °	26.2	21	63	—	—
Dimpled/protruded diameter, mm				4.40	4.40
Dimpled/protruded pitch, mm				9.86	9.86
Number of dimple/protrusion arrays				4	4

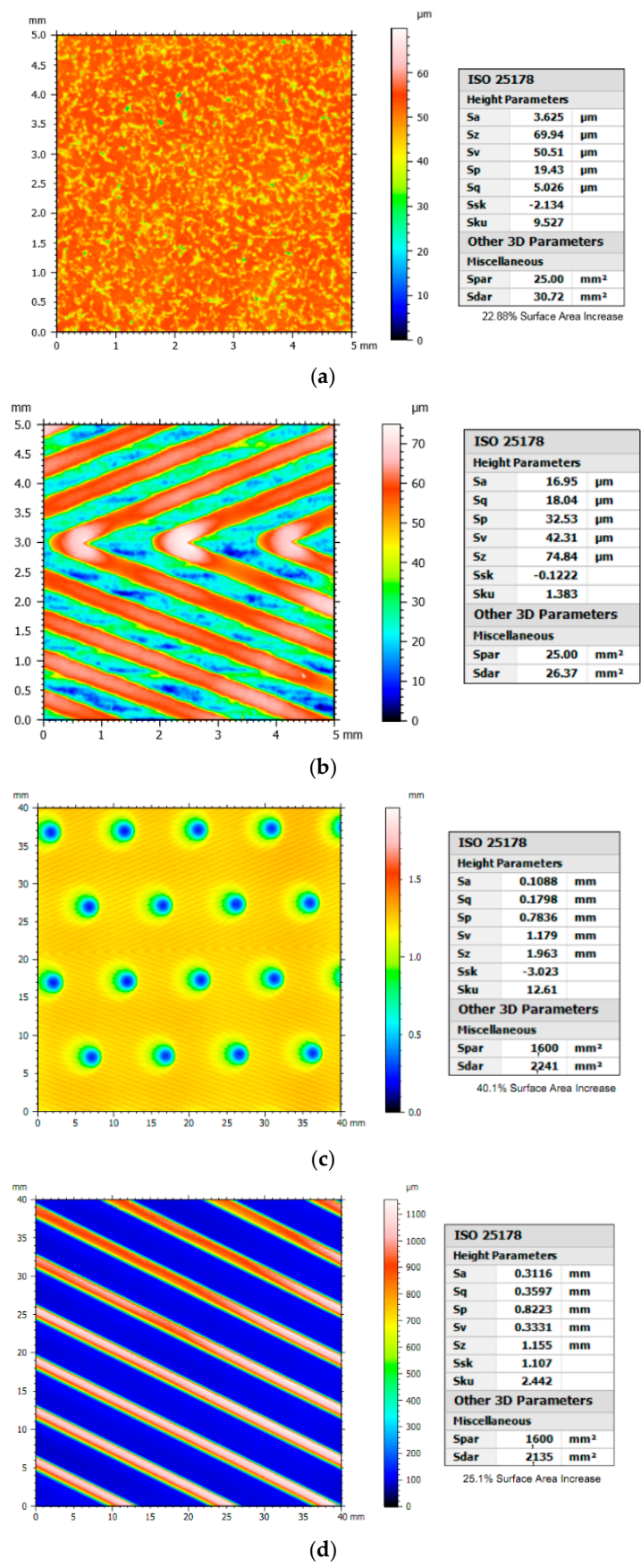


Figure 2. Cont.

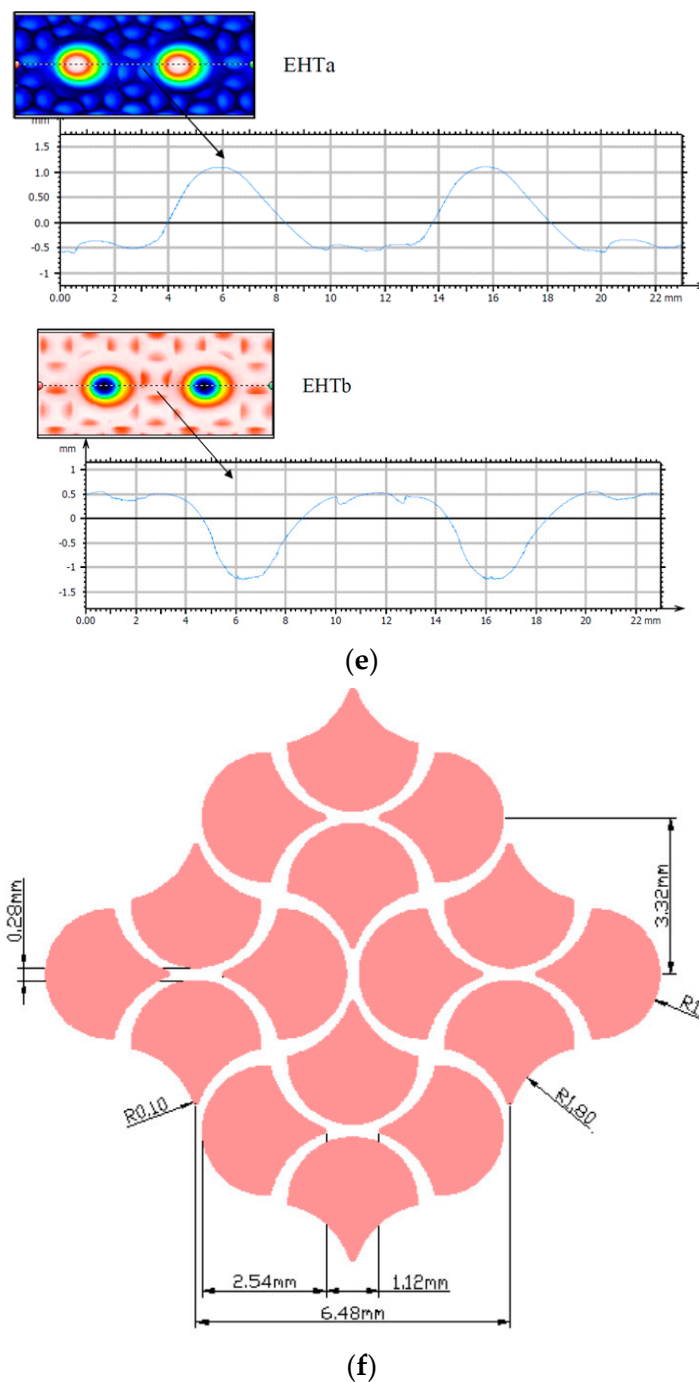


Figure 2. Surface enhancement pattern profiles and details for the following surfaces (a) Hydrophobic pattern (HY), (b) Herringbone pattern (HB), (c) Herringbone/Dimple pattern (HB/D), (d) Helical grooved pattern (HX), (e) EHT, and (f) details of the petal-shaped background pattern used in the EHT surface.

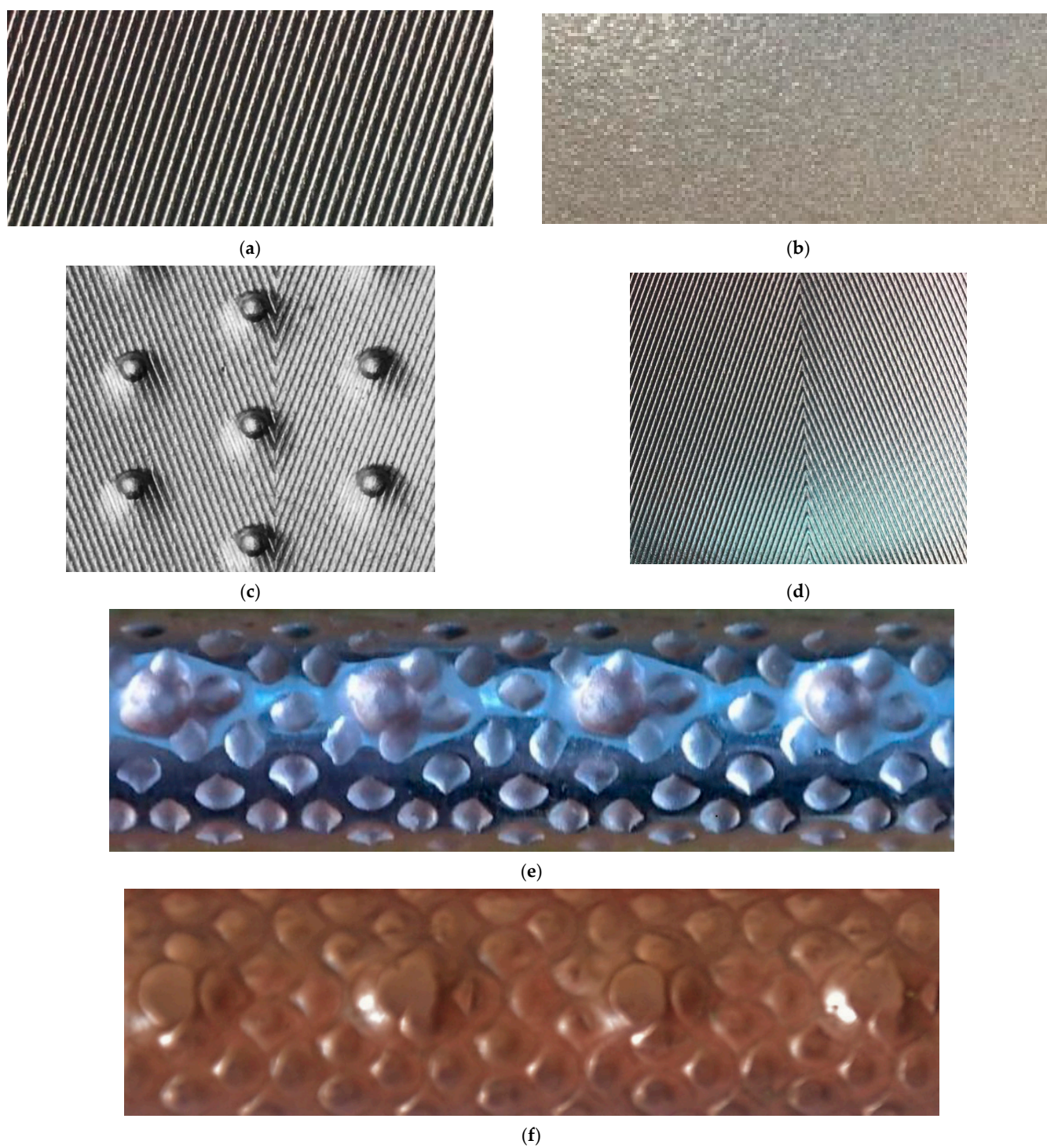


Figure 3. Images of the heat transfer surfaces that were evaluated: (a) SS-EHT-HX; (b) SS-EHT-HY; (c) SS-EHT-HB/D; (d) SS-EHT-HB; (e) Cu-EHTa; (f) Cu-EHTb.

Table 2. Accuracy of the primary and calculated parameters.

Primary Parameters	Accuracy
Diameter	±0.05 mm
Electricity	±0.1 A
Voltage	±0.1 V
Length	±0.5 mm
Temperature	±0.1 K
Range of Pressure: 0–5000 kPa	±0.075% of full scale
Range Pressure Drop: 0–50 kPa	±0.075% of full scale
Range of the Water Flowrate: 0–1000 kg/h	±0.2% of reading
Range of the Refrigerant Flowrate: 0–130 kg/h	±0.2% of reading
Calculated parameters	Accuracy
Mass flux, G_{ref} , kg/(m ² ·s)	±1.18%
Heat flux, kW/m ²	±2.65%
Vapor quality, x	±4.13%
Evaporation heat transfer coefficient, h (W/m ² ·K)	±10.55%

3. Results

3.1. Data Analysis

In order to obtain the tube-side evaporation heat transfer coefficient in enhanced tubes, the heat balance of the water flowing on the outside of the tube is used to calculate the total heat exchange capacity of the test section using Equation (1)

$$Q_{t,ts} = C_{pl,w,ts} \times m_{w,ts} \times (T_{w,ts,in} - T_{w,ts,out}) \quad (1)$$

where $m_{w,ts}$ is the water flow in the test section; $c_{pl,w,ts}$ is the average specific heat capacity of the water in the test section; $T_{w,ts,out}$ is the outlet water temperature in the test section; and $T_{w,ts,in}$ is the inlet water temperature in the test section.

The refrigerant quality at the inlet of the test section, x_{in} , is calculated from the heat exchange volume of water in the preheating section, where the total heat transfer (Equation (2)) of the refrigerant, $Q_{t,ph}$, consists of the sum of the liquid phase sensible heat (Equation (3)) of the refrigerant, Q_{sens} and the liquid-gas phase transition latent heat (Equation (4)) of the refrigerant, Q_{lat} .

$$Q_{t,ph} = C_{pl,w,ph} \times m_{w,ph} \times (T_{w,ph,in} - T_{w,ph,out}) = Q_{sens} + Q_{lat} \quad (2)$$

where $m_{w,ph}$ is the water flow in the preheating section; $c_{pl,w,ph}$ is the average specific heat capacity of the water in the preheating section; $T_{w,ph,out}$ is the outlet water temperature in the preheating section; and $T_{w,ph,in}$ is the inlet water temperature in the preheating section.

$$Q_{sens} = C_{pl,ref} \times m_{ref} \times (T_{sat} - T_{ref,ph,in}) \quad (3)$$

where m_{ref} is the mass flux rate of the refrigerant; $c_{pl,ref}$ is the average specific heat capacity of the refrigerant; T_{sat} is the saturation temperature of the refrigerant; and $T_{ref,ph,in}$ is the inlet temperature of the refrigerant in the preheating section.

Q_{lat} is calculated using

$$Q_{lat} = m_{ref} \times h_{lv} \times x_{in} \quad (4)$$

where h_{lv} is the latent heat of vaporization of the refrigerant in the preheating section.

Outlet quality x_{out} in the test section is calculated using Equation (5)

$$x_{out} = x_{in} + Q_{t,ts} / (m_{ref} \times h_{lv}) \quad (5)$$

The logarithmic mean temperature difference (LMTD) is calculated using Equation (6); it is determined using the inlet and outlet water temperatures outside the enhanced tubes and the saturation temperature of refrigerant in the tubes.

$$LMTD = \frac{(T_{w,ts,in} - T_{sat}) - (T_{w,ts,out} - T_{sat})}{\ln[(T_{w,ts,in} - T_{sat}) / (T_{w,ts,out} - T_{sat})]} \quad (6)$$

Since the evaluated enhanced tubes are brand new products that have not been used and are thoroughly cleaned before use (with cleanliness verified between runs), the fouling thermal resistance can be ignored. Tube-side evaporation heat transfer coefficient h_{ev} of the evaluated tubes can be calculated using Equation (7)

$$h_{ev} = \frac{1}{A_{ni} \left(\frac{Q_{t,ts}}{LMTD} - \frac{1}{A_o h_o} - \frac{d_o \ln(d_o/d_i)}{2k_{wall} A_o} \right)} \quad (7)$$

where A_{ni} is the actual heat transfer surface area of the evaluated tube, A_o is the outer surface area of the tube, and d_o is the outer diameter of the tube.

Previous research has demonstrated that the Gnielinski [17] correlation can be used to compute the single-phase water-side heat transfer coefficient for turbulent conditions. The deviation (between the data and the correlation) of the data (more than 800 data points) is within 20%; most of the deviations are within 10%. The applicable range of the correlation is $0.5 < Pr < 2000$ and $3000 < Re < 5 \times 10^6$. The water-side Reynolds numbers for this experiment are within the applicable range for the Gnielinski correlation. Equation (8) is the Gnielinski correlation that is used to calculate the water-side heat transfer coefficient h_o on the outside of the tubes

$$h_o = \frac{(f/2)(Re - 1000)Pr}{1 + 12.7(f/2)^{1/2}(Pr^{2/3} - 1)} \left(\frac{\mu_{bulk}}{\mu_w} \right)^{0.14} \frac{k_w}{d_h} \quad (8)$$

Fanning friction (Equation (9)) coefficient, f , is calculated using the Petukhov correlation [18] (applicable for the range $3000 < Re < 5 \times 10^6$)

$$f = (1.58 \ln Re - 3.28)^{-2} \quad (9)$$

Since the inner and outer surfaces of the test tubes are not smooth, the Gnielinski correlation can be modified using the Wilson graphic method (Equation (10)) [19]

$$\frac{1}{Ch_o} = \frac{1}{U} - \frac{d_o}{d_i h_{ev}} - \frac{d_o \ln(d_o/d_i)}{2k_{wall}} \quad (10)$$

where C is the heat transfer enhancement factor (ratio of the water-side heat transfer coefficient of the enhanced tubes to that of the smooth tubes) and U is the overall heat transfer coefficient.

The frictional pressure drop ΔP_f is calculated using Equation (11)

$$\Delta P_f = \Delta P_t - \Delta P_g - \Delta P_m - \Delta P_{se} - \Delta P_{sc} \quad (11)$$

where ΔP_t is the total pressure drop; ΔP_g is the gravity pressure drop; ΔP_m is the dynamic pressure drop; ΔP_{se} is the sudden expansion (Equation (14)) pressure drop; and ΔP_{sc} is the sudden contraction (Equation (15)) pressure drop. All evaluated tubes are placed horizontally, so ΔP_g is equal to 0.

Equation (12) is used to calculate ΔP_m [20]

$$\Delta P_m = G^2 \left\{ \left[\frac{x}{\rho_v \varepsilon} - \frac{(1-x)^2}{\rho_l (1-\varepsilon)} \right]_{out} - \left[\frac{x}{\rho_v \varepsilon} - \frac{(1-x)^2}{\rho_l (1-\varepsilon)} \right]_{in} \right\} \quad (12)$$

where G is the mass flux rate; x is the refrigerant quality; ε is the void fraction; ρ_v is the refrigerant gas density; and ρ_l is the liquid refrigerant density. Equation (13) defines ε (from Rouhani et al. [21])

$$\varepsilon = \frac{x}{\rho_v} \left\{ \left[1 + 0.12(1-x) \right] \left(\frac{x}{\rho_v} + \frac{1-x}{\rho_l} \right) + \frac{1.18(1-x) \left[g\sigma(\rho_l - \rho_v)^{0.25} \right]}{G\rho_l^{0.5}} \right\}^{-1} \quad (13)$$

Finally, ΔP_{se} and ΔP_{sc} are calculated by formulas (14) and (15), respectively [22,23]

$$\Delta P_{se} = \frac{G^2 \zeta (1 - \zeta)}{\rho_l} \left[1 - \left(\frac{\rho_l - \rho_v}{\rho_v} \right) \right] \quad (14)$$

$$\Delta P_{sc} = \frac{G^2}{2\rho_l} \left[1 - \left(\frac{\rho_l - \rho_v}{\rho_v} \right) \right] \quad (15)$$

where ζ is the area ratio.

3.2. Evaluation of Smooth Tube Evaporation Heat Transfer Correlations

Fang [24], Liu et al. [25], and Gungor et al. [26] proposed evaporation heat transfer correlations for smooth tubes. Convective evaporation heat transfer is assumed to consist of forced convection and nucleate boiling in the Fang [24] and Liu et al. [25] models. In the Gungor et al. [26] model, the evaporation heat transfer coefficient is the sum of these two components, while in the Liu et al. [25] model, the evaporation heat transfer coefficient is obtained from the square roots of these two parts. Finally, the dimensionless number Fa is used in the Fang [24] model in order to predict the evaporation heat transfer coefficient.

Figure 4 compares the deviations between the evaporation heat transfer values derived using the three smooth tube correlations and experimental data; all deviations are within $\pm 20\%$, with the highest accuracy being predicted by the Liu et al. [25] model.

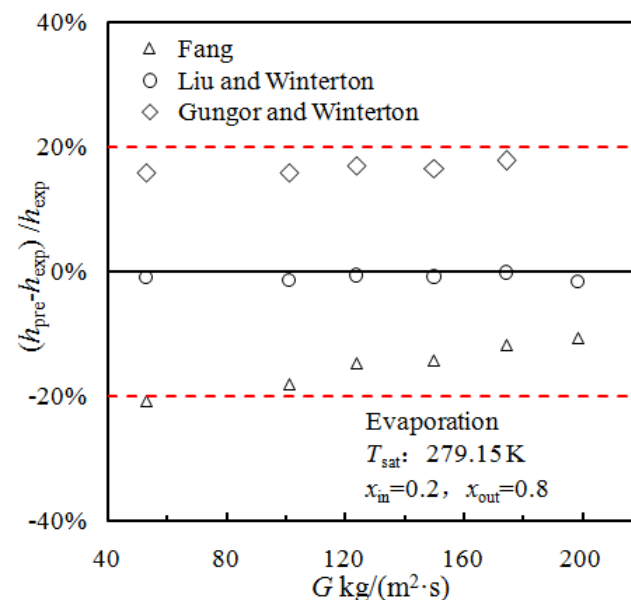


Figure 4. Comparison of deviations from experimental data and values predicted using various smooth tube evaporation correlations.

3.3. Heat Transfer Enhanced Factor (EF) for Enhanced Tubes

In order to compare the evaporation heat transfer coefficient in two-sided enhanced tubes, a heat transfer enhancement factor (EF_h) is presented in Equation (16). It is defined as the ratio of the HTC of an enhanced tube to the HTC of a smooth tube under the same working conditions

$$EF_h = h_e / h_s \quad (16)$$

where h_e is the heat transfer coefficient of an enhanced tube and h_s is the heat transfer coefficient of a smooth tube.

Figure 5 compares the heat transfer enhancement factor of the enhanced tubes that were evaluated in this study. The heat transfer enhanced factor of the Cu-EHTb tube is the highest, followed by the SS-EHT-HB/HY, SS-EHT-HX, Cu-EHTa, SS-EHT-HB, and SS-EHT-HB/D tubes; some tubes do not improve heat transfer. For the Cu-EHTa, Cu-EHTb, and SS-EHT-HB/D tubes, the heat transfer factor shows a downward trend, while for the SS-EHT-HB/HY, SS-EHT-HX, and SS-EHT-HB tubes, there is an upward trend. When the mass flux rate is lower than $150 \text{ kg/m}^2\text{s}$, the Cu-EHTb provides the best enhancement.

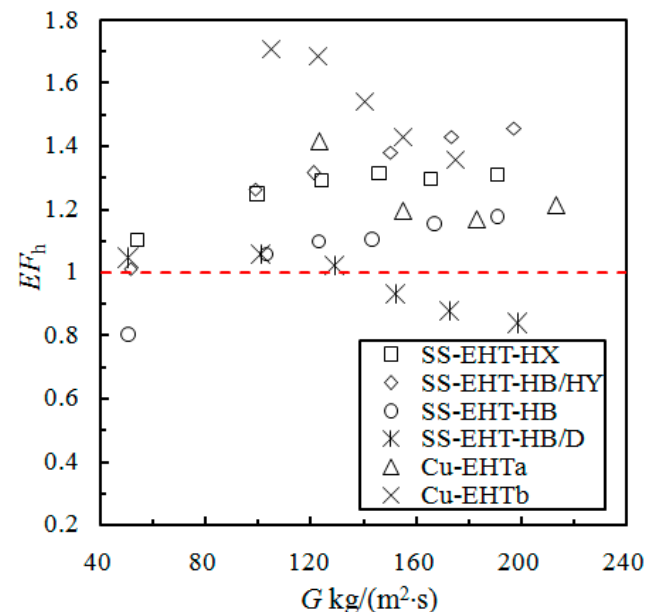


Figure 5. Comparison of the evaporation heat transfer enhancement factors (EF) for the enhanced tubes from this study.

For Cu-EHTa and Cu-EHTb, the enhancement characters that make up the surface increase: (i) the wetting perimeter; (ii) the effective heat transfer surface area; and (iii) the axial velocity (produced by the protruding surface character acting as an obstruction to the fluid flow). In addition, channels between the petal arrays (see Figures 2f and 3e,f) form a tight network that produces a large number of nucleating points where stable bubbles form and try to grow. Stable bubbles can continue to grow in pits and in the small petal-shaped cavities on the inner surface of the Cu-EHTb tube; this accelerates the formation of slender bubbles. Additionally, the bubble nucleation process is shortened, and small bubbles are quickly washed away from the inner surface and separated by the surface array of raised petals. Therefore, the Cu-EHTb tube has a longer forced convective boiling heat transfer section in which the liquid film is thinner, and the Cu-EHTb outperforms most of the tubes for the range of conditions considered.

The size of the dimple enhancement on the surface of the SS-EHT-HB/D is large and reduces the regions of nucleate boiling. Additionally, it provides a disturbance of the fluid during the forced convection process; this results in a lower heat transfer coefficient than found in smooth tubes. Greater heat transfer enhancement is obtained using the composite structure of the hydrophobic pattern and the HB pattern (SS-EHT-HB/HY); this combination increases the number of nucleation points; additionally, it increases the fluid disturbance and the intensity of the turbulence. Finally, average performance is obtained from the SS-EHT-HX and SS-EHT-HB tubes; these structures increase fluid disturbance but do not increase the number of nucleation sites; therefore, optimum enhanced heat transfer factors are not achieved.

3.4. Evaluation of Heat Transfer Enhancement

Performance factor (PF), a dimensionless parameter, is made up of the enhanced heat transfer factor (Equation (16)) multiplied by the pressure drop ratio and is given in Equation (17)

$$PF = (h_e/h_s) \times (p_s/p_e) \quad (17)$$

where p_e is the pressure drop of the enhanced tubes and p_s is the pressure drop of the smooth tubes under the same working conditions. Use of the PF factor provides additional insight into the performance of the tube.

Figure 6 presents the PF of different enhanced tubes; when the mass flux rate is higher than $100 \text{ kg}/(\text{m}^2 \cdot \text{s})$, the PF of the SS-EHT-HB/HY and the SS-EHT-HX tubes are all greater than 1, while the PF of the SS-EHT-HB/D, Cu-EHTa, and Cu-EHTb tubes are less than 1. When the mass flux rate is lower than $100 \text{ kg}/(\text{m}^2 \cdot \text{s})$, the PF of all the enhanced tubes is less than 1; with an increasing mass flux rate, the PF increases for the SS-EHT-HB/HY, SS-EHT-HX, and SS-EHT-HB tubes, but decreases for the PF of the HB/D tube. Finally, the PF of the Cu-EHTa and Cu-EHTb tubes increases slowly.

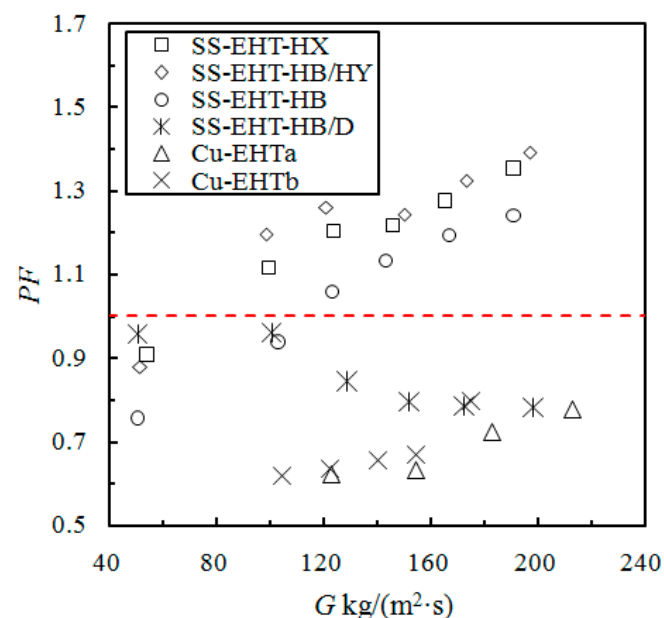


Figure 6. Comparison of the evaporation heat transfer performance factors (PF) of evaporation heat transfer in the enhanced tubes.

The best overall evaporation heat transfer performance is demonstrated by the SS-EHT-HB/HY and SS-EHT-HX tubes, followed by the SS-EHT-HB tube and the SS-EHT-HB/D tube; the Cu-EHTa and Cu-EHTb tubes have the worst overall performance (even worse than smooth tubes). When looking at the Cu-EHTa and Cu-EHTb tubes, it can be seen that there is an increase in the number of nucleation sites, and the enhancement characters produce a fluid disturbance; however, the increase in the pressure drop outweighs the increase in the heat transfer coefficient.

3.5. Evaluation of Evaporation Correlations for Enhanced Tubes

Several previous studies have proposed tube-side evaporation heat transfer models for smooth tubes; Liu et al. [21] and Gungor et al. [26] have proposed correlations that use enhancing and inhibiting factors in order to improve the convective boiling and nucleate boiling terms. Kandlikar [27] proposed a correlation that determines whether the flow is convection boiling or nucleate boiling based on Co and Fr_{10} ; in order to improve prediction accuracy, they introduce the parameter f_{fl} —a parameter that is based on the working medium type. However, the above correlations are all based on smooth tubes; in order to

consider the use of these correlations, they must first be evaluated for use with enhanced tubes. Figure 7 shows deviations (between experimental data and values predicted using different correlations) for the enhanced tubes considered in this study.

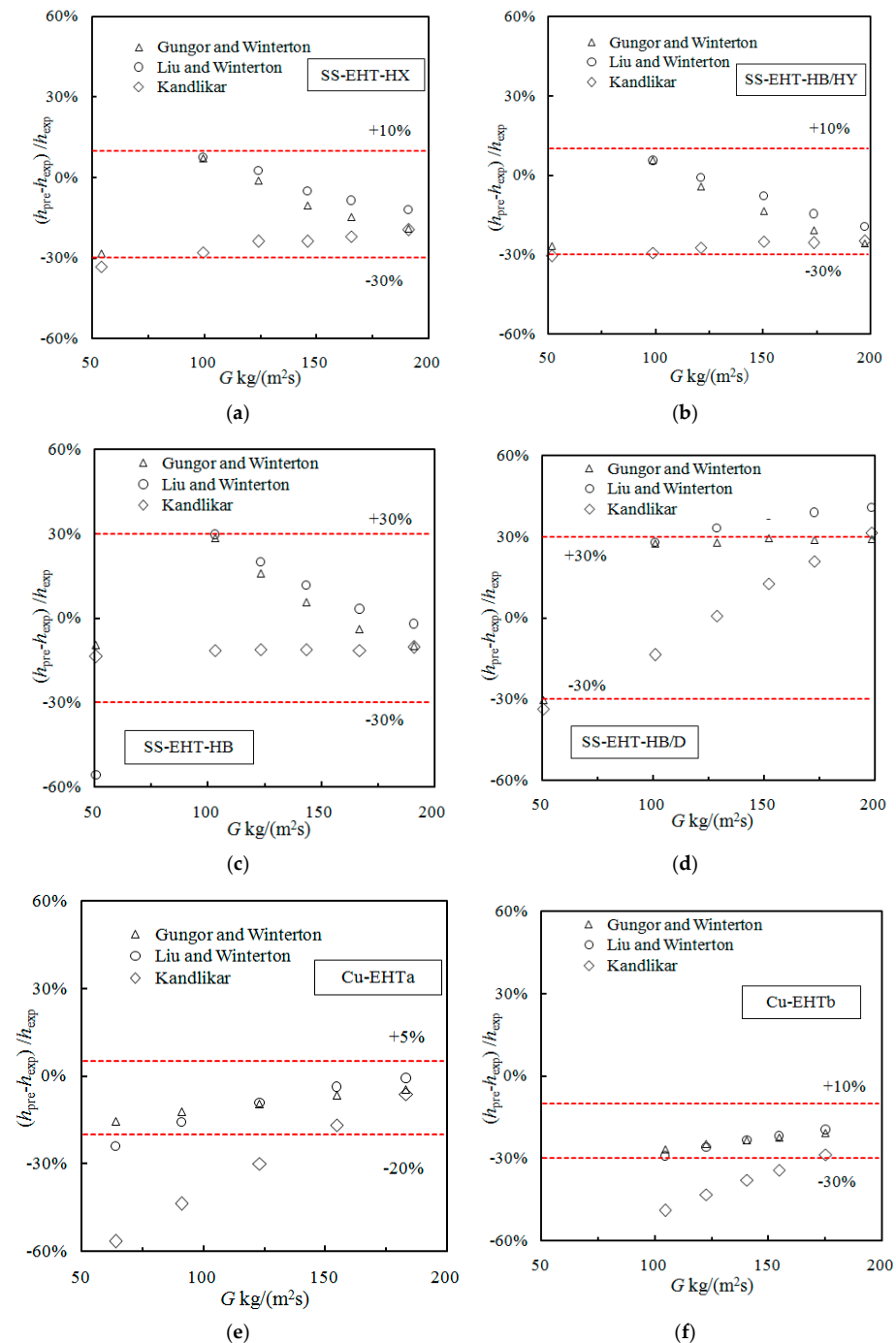


Figure 7. Comparison of the deviation of experimental data and values predicted using different smooth tube correlations for enhanced tubes. (a) Comparison of deviations of experimental data and values predicted using different correlations for SS-EHT-HX tubes; (b) Comparison of deviations of experimental data and values predicted using different correlations for SS-EHT-HB/HY tubes; (c) Comparison of deviations of experimental data and values predicted using different correlations for SS-EHT-HB tubes; (d) Comparison of deviations of experimental data and values predicted using different correlations for SS-EHT-HB/D tubes; (e) Comparison of deviations of experimental data and values predicted using different correlations for Cu-EHTa tubes; (f) Comparison of deviations of experimental data and values predicted using different correlations for Cu-EHTb tubes.

As shown in Figure 7, the predicted trends of the three correlations for the SS-EHT-HX and SS-EHT-HB/HY tubes demonstrate the same trend as they did for the heat transfer enhancement factor (EF_h). Low values are predicted for the SS-EHT-HX, SS-EHT-HB/HY, Cu-EHTa, and Cu-EHTb tubes when using these three smooth tube correlations to predict enhanced tube performance; however, high values are predicted for the SS-EHT-HB/D tube. This is contrary to the heat transfer enhancement factor trend (EF_h) for this tube. In general, the higher the measured heat transfer coefficient, the lower the predicted value. In summary, Gungor et al. [26] predict that 94.3% of data points are within $\pm 30\%$; Kandlikar [27] and Liu et al. [25] both predict that 68.6% of data points are within $\pm 30\%$. Based upon this accuracy, the existing correlations are not suitable for guiding engineering design because the predicted enhanced tube value of evaporation heat transfer deviates greatly from the measured values of the enhanced tubes. As a result, the existing correlations must be modified so that they are applicable for use with enhanced tubes and the deviation is within an acceptable range. Figure 8 presents a comparison of the deviation of the experimental data and the values predicted using correlations modified for use with enhanced tubes. Table 3 details the modified correlations.

Table 3. Modified correlation.

Authors	Correlation
Modified Kandlikar correlation	$\frac{h_{TP}}{h_l} = C_1 Co^{C_2} (25 Fr_{lo})^{C_5} + C_3 Bo^{C_4} F_{fl}$ $h_l = 0.023 Re_l^{0.8} Pr_l^{0.4} k_l / d$ $Co = \left(\frac{1-x}{x} \right)^{0.8} \left(\frac{\rho_v}{\rho_l} \right)^{0.5}$ $Bo = \frac{q}{G h_{fg}}, Fr_{lo} = \frac{G^2}{\rho_l^2 g d}$ <p>Convective region: $C_1 = 1.1360$, $C_2 = -0.9$, $C_3 = 667.2$, $C_4 = 0.7$, $C_5 = 0.3$ Nucleate boiling region: $C_1 = 0.6683$, $C_2 = -0.2$, $C_3 = 1058.0$, $C_4 = 0.7$, $C_5 = 0.3$ F_{fl} depends on tube type: (i) SS-EHT-HX, $F_{fl} = 2.10$; (ii) SS-EHT-HB/HY, $F_{fl} = 2.05$; (iii) SS-EHT-HB, $F_{fl} = 1.58$;</p> $\frac{h_{TP}}{h_l} = \text{MAX}(\text{Nucleate Boiling Term}, \text{Convective Boiling Term})$ <p>Applicable for SS-EHT-HX, SS-EHT-HB/HY, and SS-EHT-HB tubes.</p>
Modified Gungor and Winterton correlation	$h_{tp} = B(Eh_l + Sh_{pool})$ $h_{pool} = 55 P_r^{0.12} (-\log_{10} P_r)^{-0.55} M^{-0.5} q^{0.67}$ $E = 1 + 24000 Bo^{1.16} + 1.37 \left(\frac{1}{X_{tt}} \right)^{0.86}$ $S = \frac{1}{1 + 1.15 \times 10^{-6} E^2 Re_l^{1.17}}$ $X_{tt} = \left(\frac{1-x}{x} \right)^{0.9} \left(\frac{\rho_v}{\rho_l} \right)^{0.5} \left(\frac{\mu_l}{\mu_v} \right)^{0.1}$ $Fr = \frac{G^2}{\rho_l^2 g d}$ <p>If $Fr \leq 0.05$, E is multiplied by E_2, $E_2 = Fr^{(0.1-2Fr)}$ S need multiplied by S_2, $S_2 = Fr^{0.5}$ B depends on tube type: (i) SS-EHT-HB/D, $B = 0.72$; (ii) Cu-EHTa, $B = 1.11$; (iii) Cu-EHTb, $B = 1.31$.</p> <p>Applicable for SS-EHT-HB/D, Cu-EHTa, Cu-EHTb</p>

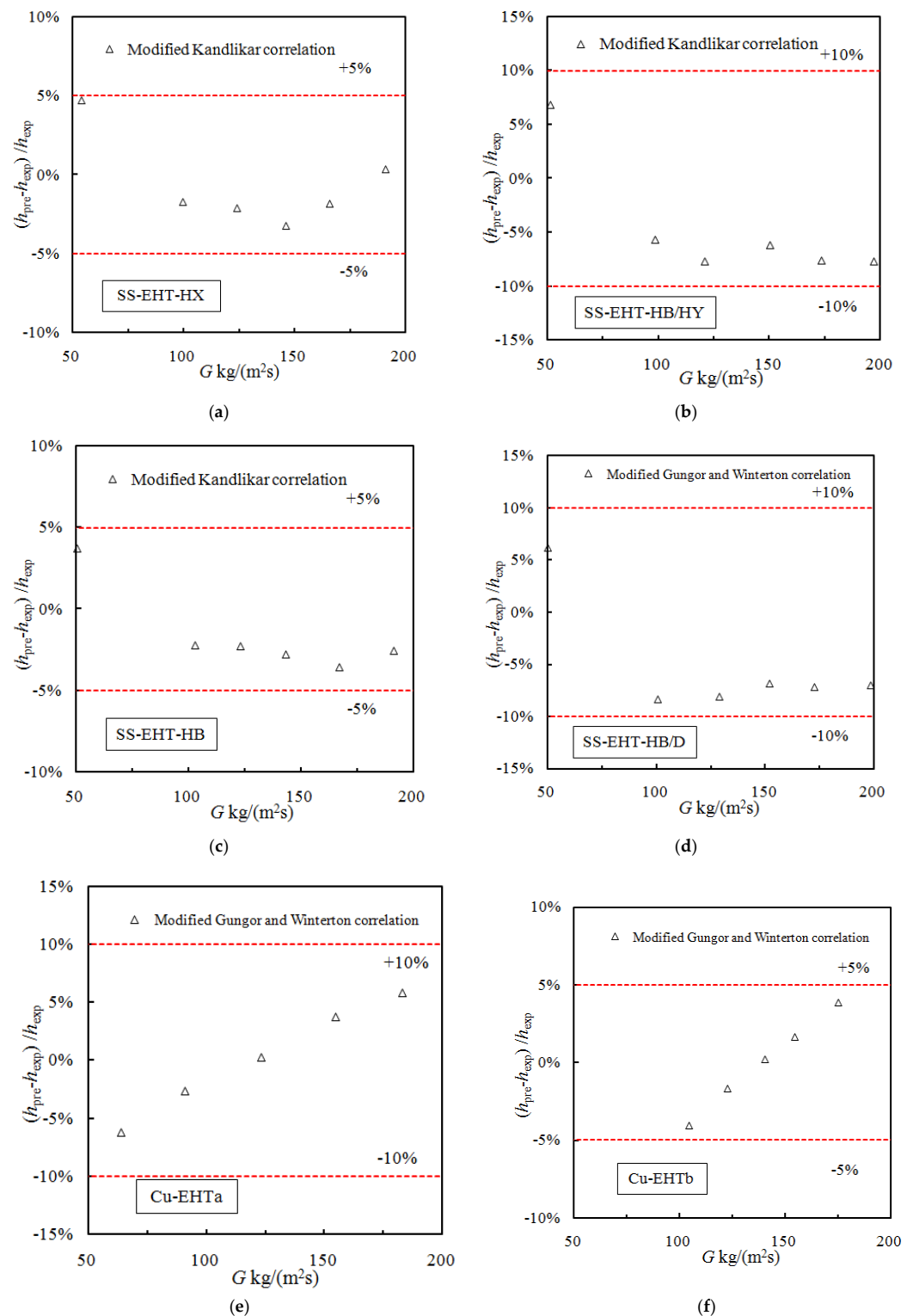


Figure 8. Comparison of the deviation of experimental data and values predicted using modified smooth tube models that can be used for enhanced tubecorrelations. (a) Prediction effect of the modified Kandlikar correlation for the SS-EHT-HX tube; (b) Prediction effect of the modified Kandlikar correlation for the SS-EHT-HB/HY tube; (c) Prediction effect of the modified Kandlikar correlation for the SS-EHT-HB tube; (d) Prediction effect of the modified Gungor and Winterton correlation for the SS-EHT-HB/D tube; (e) Prediction effect of the modified Gungor and Winterton correlation for the Cu-EHTa tube; (f) Prediction effect of the modified Gungor and Winterton correlation for the Cu-EHTb tube.

The deviation of the experimental data and values predicted using the modified Gungor and Winterton correlation (see Table 3) and the modified Kandlikar correlation (see Table 3) for the evaporation heat transfer coefficient in enhanced tubes is within $\pm 10\%$ of the standard deviation (see Figure 8).

3.6. Thermal Resistance Evaluation

Figures 9 and 10 compare the proportion of thermal resistance in the 12.7 mm outer diameter (OD) (see Figure 9) and the 9.52 mm OD (see Figure 10) enhanced tubes. In Figure 10, the data for the 9.52 mm OD SS-4LB tube, the 9.52 mm OD SS-1EHT1 tube, and the 9.52 mm OD SS-1EHT2 tube are from Shen et al. [15]; the data for the 9.52 mm OD Cu-EHTa and 9.52 mm OD Cu-EHTb tubes are from Sun et al. [13].

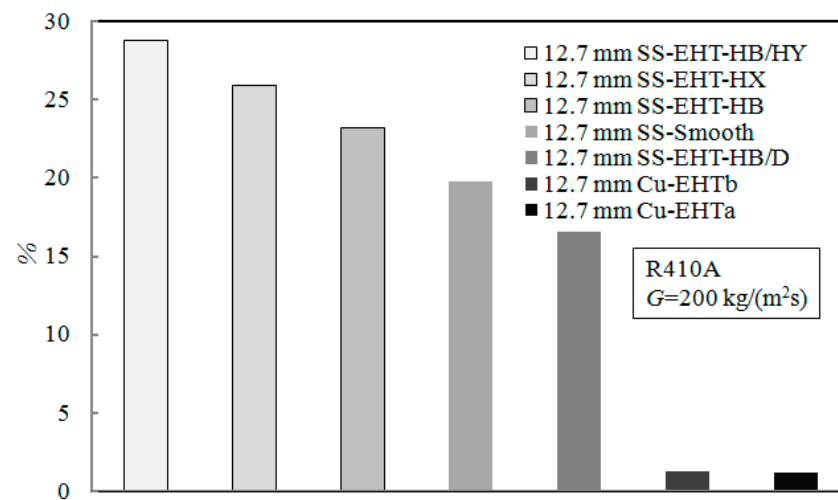


Figure 9. Comparison of thermal resistance (for various tube types based upon data obtained in this study) to total evaporation thermal resistance for 12.7 mm OD tubes.

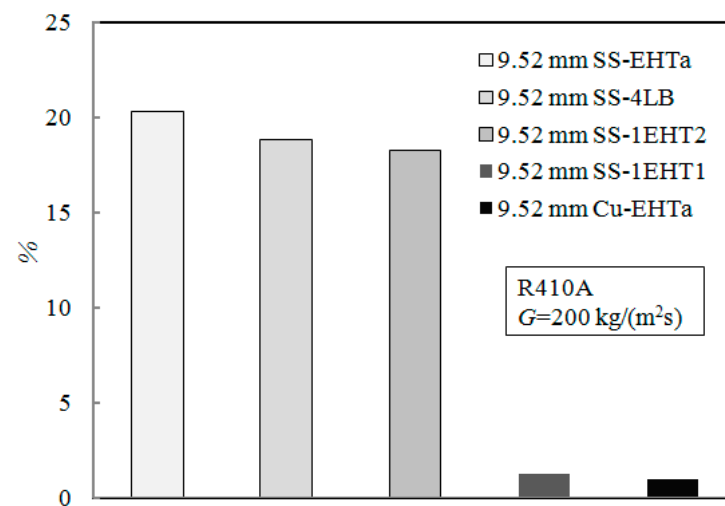


Figure 10. Comparison of thermal resistance (for various tube types) to total evaporation thermal resistance for 9.52 mm OD tubes. Data of the 9.52 mm OD SS-4LB tube, 9.52 mm OD SS-1EHT1 tube and 9.52 mm OD SS-1EHT2 tube are from K Shen et al. [15]; data of the 9.52 mm OD Cu-EHTa tube and 9.52 mm OD Cu-EHTb tube are data are from Sun et al. [13].

Wall thermal resistance is the conductive thermal resistance of the tube wall; total evaporation thermal resistance (shown as part of Equation (7)) is the total thermal resistance. It can be seen from Figure 9 that the wall thermal resistance of the 12.7 mm OD stainless steel tube is approximately 15% of the total evaporation heat transfer resistance; this is in

contrast to the wall thermal resistance of a copper tube, which is less than 1.5% of the total evaporation heat transfer resistance. It can be seen from Figure 10 that the wall thermal resistance of the 9.52 mm stainless steel tube exceeds 18% of the overall evaporation heat transfer resistance, while the thermal wall resistance of the copper tube is less than 1.5% of the evaporation heat transfer resistance. For 12.7 mm and 9.52 mm tube types, the influence of stainless steel materials on evaporation heat transfer cannot be ignored, while copper wall materials produce much less thermal wall resistance.

4. Conclusions

The evaporation heat transfer of R410a in smooth tubes and enhanced tubes was investigated experimentally in this study. Conditions include an evaporation saturation temperature of 6 °C, an inlet quality of 0.2, and an outlet quality of 0.8. Changes in the evaporation heat transfer coefficient and pressure drop as a function of mass flux rate were measured. The following findings are made:

- (1) The enhanced heat transfer factor (EF) of the Cu-EHTb tube is the highest, and it is closely related to increasing the number of nucleation points. This contrasts with the enhanced heat transfer factor of the SS-EHT-HB/D tube, which is the lowest (even lower than that of smooth tubes). This is the result of the dimple pattern being large, resulting in a reduction in the number of nucleation points; the fluid disturbance reduces the HTC. The trend of the enhanced heat transfer factor (EF) is different for different tubes.
- (2) The best overall evaporation heat transfer characteristics are seen in the SS-EHT-HB/HY and SS-EHT-HX tubes, with the *PF* always greater than 1. Performance of the SS-EHT-HB/D, Cu-EHTa and Cu-EHTb tubes are the worst (for most conditions smooth tubes perform better), with the *PF* less than 1. With increasing mass flux rate, the *PF* of the SS-EHT-HB/HY, SS-EHT-HX, and SS-EHT-HB tubes all increase, while the *PF* of the SS-EHT-HB/D tube decreases. Finally, the *PF* of the Cu-EHTa and Cu-EHTb tubes increases slowly.
- (3) Correlations are used to predict the evaporation heat transfer coefficient of enhanced tubes; when using the unmodified model, the deviation of the data points is greater than $\pm 30\%$; however, when using the modified versions of the (i) Gungor et al. correlation and (ii) the Kandlikar correlation results, the heat transfer coefficient can be predicted within $\pm 10\%$ of the enhanced tube data.
- (4) A comparison of tube materials was performed for 12.7 mm and 9.52 mm OD tubes; it was determined that stainless steel materials contribute more than 15% of the total evaporation heat transfer resistance; however, for copper tubes, the percentage of resistance is less than 2%.

Author Contributions: Conceptualization, W.L.; Data curation, X.-Z.L., W.F., X.-B.W. and Z.-P.W.; Formal analysis, X.W.; Investigation, X.-Z.L., W.F., X.-B.W. and Z.-P.W.; Methodology, X.W.; Project administration, W.L.; Resources, W.L.; Validation, X.-Z.L., W.F. and X.-B.W.; Writing—original draft, X.W.; Writing—review & editing, D.J.K. All authors have read and agreed to the published version of the manuscript.

Funding: This research was funded by the National Science Foundation of China (52076187).

Data Availability Statement: The pre-processed data used in this study are available on request from the corresponding author.

Conflicts of Interest: The authors declare no conflict of interest.

Nomenclature

A	test tube surface area, m ²
Bo	boiling number = q/Gh_{lv}
C	enhancement ratio
Co	convection number = $\left(\frac{1-x}{x}\right)^{0.8} \left(\frac{\rho_v}{\rho_l}\right)^{0.5}$
c_p	specific heat, J/(kg·K)
D	dimple
d	test tube diameter, m
d_h	hydraulic diameter, m
E	enhancement factor
ev	evaporation
Fa	$(\rho_l - \rho_v) \sigma / G^2 D_h$
f	Fanning friction factor
F_{fl}	fluid-dependent parameter
Fr	Froude number
Fr_{lo}	Froude number with all flow as liquid = $G^2 / (\rho_l^2 g D)$
G	mass flux, kg/(m ² ·s)
g	gravitational acceleration, m/s ²
HB	herringbone
HB/D	herringbone dimple
HB/HY	hydrophobic herringbone
HX	spiral microgrooves
h	heat transfer coefficient, W/(m ² ·K)
h_{lv}	latent heat of vaporization, J/kg
k	thermal conductivity, W/(m·K)
l	liquid only
L	tube length, m
$LMTD$	logarithmic mean temperature, K
m	mass flux, kg/s
M	molecular weight
P	Pressure, kpa
PF	performance factor
Pr	Prandtl number
Q	heat transfer amount, W
q	heat flux, W/m ²
Re	Reynolds number
S	suppression factor
Sa	arithmetical mean height, mm
Sq	root mean square height, mm
Sp	maximum peak height, mm
Sv	maximum pit height, mm
Sz	maximum height, mm
Ssk	skewness
Sku	kurtosis
S_{par}	projected area, mm ²
S_{dar}	developed area, mm ²
T/t	temperature, K/°C
U	Total heat transfer coefficient, W/(m ² ·K)
x	vapor quality
X_{tt}	Martinelli parameter $X_{tt} = \left(\frac{1-x}{x}\right)^{0.9} \left(\frac{\rho_v}{\rho_l}\right)^{0.5} \left(\frac{\mu_l}{\mu_v}\right)^{0.1}$
<i>Greek symbols</i>	
μ	dynamic viscosity, Pa·s
ρ	density, kg/m ³
ε	void fraction
σ	surface tension, N/m
ζ	area ratio

Subscripts

<i>bulk</i>	bulk temperature
<i>exp</i>	experimental
<i>f</i>	frictional
<i>g</i>	gravitational
<i>i</i>	inner
<i>in</i>	inlet
<i>l</i>	liquid phase
<i>lat</i>	latent heat
<i>m</i>	momentum
<i>ni</i>	actual heat transfer area
<i>o</i>	outer
<i>out</i>	outlet
<i>ph</i>	preheating section
<i>pool</i>	pool boiling
<i>pre</i>	predictive
<i>r</i>	reduced
<i>ref</i>	refrigerant
<i>s</i>	smooth
<i>sat</i>	saturated
<i>sc</i>	sudden contraction
<i>se</i>	sudden enlargement
<i>sens</i>	sensible heat
<i>t</i>	total
<i>te</i>	test section
<i>tp</i>	two-phase
<i>ts</i>	test section
<i>v</i>	vapor phase
<i>wall</i>	wall parameters
<i>w</i>	water

References

- Kim, Y.; Seo, K.; Chung, J.T. Evaporation heat transfer characteristics of R-410A in 7 and 9.52 mm smooth/micro-fin tubes. *Int. J. Refrig.* **2002**, *25*, 716–730. [\[CrossRef\]](#)
- Wellsandt, S.; Vamling, L. Evaporation of R134a in a horizontal herringbone microfin tube: Heat transfer and pressure drop. *Int. J. Refrig.* **2005**, *28*, 889–900. [\[CrossRef\]](#)
- Wu, Z.; Wu, Y.; Sundén, B.; Li, W. Convective vaporization in micro-fin tubes of different geometries. *Exp. Therm. Fluid Sci.* **2013**, *44*, 398–408. [\[CrossRef\]](#)
- Yang, C.M.; Hrňjak, P. A new flow pattern map for flow boiling of R410a in horizontal micro-fin tubes considering the effect of the helix angle. *Int. J. Refrig.* **2020**, *109*, 154–160. [\[CrossRef\]](#)
- Rollmann, P.; Spindler, K. New models for heat transfer and pressure drop during flow boiling of R407C and R410A in a horizontal microfin tube. *Int. J. Therm. Sci.* **2016**, *103*, 57–66. [\[CrossRef\]](#)
- Webb, R.L.; Kim, N.-H. *Principles of Enhanced Heat Transfer*, 2nd ed.; CRC Press: Boca Raton, FL, USA, 2005; pp. 320–400.
- Vicente, P.G.; García, A.; Viedma, A. Heat transfer and pressure drop for low Reynolds turbulent flow in helically dimpled tubes. *Int. J. Heat Mass Transf.* **2002**, *45*, 543–553. [\[CrossRef\]](#)
- Kukulka, D.J.; Smith, R. Thermal-hydraulic performance of Vipertex 1EHT enhanced heat transfer tubes. *Appl. Therm. Eng.* **2013**, *61*, 60–66. [\[CrossRef\]](#)
- Guo, S.P.; Wu, Z.; Li, W.; Kukulka, D.; Sundén, B.; Zhou, X.P.; Wei, J.J.; Simon, T. Condensation and evaporation heat transfer characteristics in horizontal smooth, herringbone and enhanced surface EHT tubes. *Int. J. Heat Mass Transf.* **2015**, *85*, 281–291. [\[CrossRef\]](#)
- Kukulka, D.J.; Smith, R.; Li, W. Comparison of tubeside condensation and evaporation characteristics of smooth and enhanced heat transfer 1EHT tubes. *Appl. Therm. Eng.* **2015**, *89*, 1079–1086. [\[CrossRef\]](#)
- Shafae, M.; Mashouf, H.; Sarmadian, A.; Mohseni, S.G. Evaporation heat transfer and pressure drop characteristics of R-600a in horizontal smooth and helically dimpled tubes. *Appl. Therm. Eng.* **2016**, *107*, 28–36. [\[CrossRef\]](#)
- Li, W.; Chen, J.; Zhu, H.; Kukulka, D.J.; Minkowycz, W.J. Experimental study on condensation and evaporation flow inside horizontal three dimensional enhanced tubes. *Int. Commun. Heat Mass Transf.* **2017**, *80*, 30–40. [\[CrossRef\]](#)
- Sun, Z.C.; Li, W.; Ma, X.; Ma, L.X.; Yan, H. Two-phase heat transfer in horizontal dimpled/protruded surface tubes with petal-shaped background patterns. *Int. J. Heat Mass Transf.* **2019**, *140*, 837–851. [\[CrossRef\]](#)

14. Zheng, B.; Wang, J.; Guo, Y.; Kukulka, D.J.; Tang, W.; Smith, R.; Sun, Z.; Li, W. An Experimental Study of In-Tube Condensation and Evaporation Using Enhanced Heat Transfer (EHT) Tubes. *Energies* **2021**, *14*, 867. [\[CrossRef\]](#)
15. Shen, K.; Sun, Z.; Yan, X.; Li, W.; Kukulka, D.J.; Zhou, J. Comparison of Evaporation and Condensation Characteristics among Three Enhanced Tubes. In Proceedings of the ASME 2018 International Technical Conference and Exhibition on Packaging and Integration of Electronic and Photonic Microsystems, San Francisco, CA, USA, 27–30 August 2018.
16. Moffat, R.J. Describing the uncertainties in experimental results. *Exp. Therm. Fluid Sci.* **1988**, *1*, 3–17. [\[CrossRef\]](#)
17. Gnielinski, V. New Equations for Heat and Mass Transfer in Turbulent Pipe and Channel Flow. *Int. Chem. Eng.* **1976**, *16*, 8–16.
18. Petukhov, B.S. Heat transfer and friction in turbulent pipe flow with variable physical properties. *Adv. Heat Transf.* **1970**, *6*, 503–564.
19. Wilson, E.E. A Basis for Rational Design of Heat Transfer Apparatus. *J. Heat Transf. Trans. ASME* **1915**, *37*, 47–82.
20. Collier, J.G. *Convective Boiling and Condensation*, 2nd ed.; Mc Graw-Hill International Book Co: London, UK; New York, NY, USA, 1981.
21. Rouhani, S.Z.; Axelsson, E. Calculation of void volume fraction in the subcooled and quality boiling regions. *Int. J. Heat Mass Transf.* **1970**, *13*, 383–393. [\[CrossRef\]](#)
22. Chisholm, D.; Sutherland, L.A. Prediction of Pressure Gradients in Pipeline Systems during Two-Phase Flow. *Proc. Inst. Mech. Eng.* **1969**, *184*, 24–32. [\[CrossRef\]](#)
23. McGee, J.W. *Two-Phase Flow through Abrupt Expansions and Contractions*; North Carolina State University: Raleigh, NC, USA, 1966.
24. Fang, X. A new correlation of flow boiling heat transfer coefficients based on R134a data. *Int. J. Heat Mass Transf.* **2013**, *66*, 279–283. [\[CrossRef\]](#)
25. Liu, Z.; Winterton, R.H.S. A general correlation for saturated and subcooled flow boiling in tubes and annuli, based on a nucleate pool boiling equation. *Int. J. Heat Mass Transf.* **1991**, *34*, 2759–2766. [\[CrossRef\]](#)
26. Gungor, K.E.; Winterton, R. A general correlation for flow boiling in tubes and annuli. *Int. J. Heat Mass Transf.* **1986**, *29*, 351–358. [\[CrossRef\]](#)
27. Kandlikar, G. A General Correlation for Saturated Two-Phase Flow Boiling Heat Transfer Inside Horizontal and Vertical Tubes. *J. Heat Transf.* **1990**, *112*, 219–228. [\[CrossRef\]](#)

Disclaimer/Publisher’s Note: The statements, opinions and data contained in all publications are solely those of the individual author(s) and contributor(s) and not of MDPI and/or the editor(s). MDPI and/or the editor(s) disclaim responsibility for any injury to people or property resulting from any ideas, methods, instructions or products referred to in the content.